SCIENTIFIC REPORTS

OPEN

SUBJECT AREAS:
ELECTRONIC AND SPINTRONIC DEVICES
ELECTRONIC DEVICES

Received
30 September 2014

Accepted
20 November 2014

Published
8 December 2014

Correspondence and requests for materials should be addressed to W.B.M. (miwenbo@tju.edu.cn) or U.S. (Udo.Schwingenschlogl@kaust.edu.sa)

The Interface between Gd and Monolayer MoS_2: A First-Principles Study

Xuejing Zhang[1], Wenbo Mi[1], Xiaocha Wang[2], Yingchun Cheng[3] & Udo Schwingenschlögl[3]

[1]Tianjin Key Laboratory of Low Dimensional Materials Physics and Preparation Technology, Faculty of Science, Tianjin University, Tianjin 300072, China, [2]Tianjin Key Laboratory of Film Electronic & Communicate Devices, School of Electronics Information Engineering, Tianjin University of Technology, Tianjin 300191, China, [3]PSE Division, KAUST, Thuwal 23955-6900, Kingdom of Saudi Arabia.

We analyze the electronic structure of interfaces between two-, four- and six-layer Gd(0001) and monolayer MoS_2 by first-principles calculations. Strong chemical bonds shift the Fermi energy of MoS_2 upwards into the conduction band. At the surface and interface the Gd *f* states shift to lower energy and new surface/interface Gd *d* states appear at the Fermi energy, which are strongly hybridized with the Mo 4*d* states and thus lead to a high spin-polarization (ferromagnetically ordered Mo magnetic moments of 0.15 μ_B). Gd therefore is an interesting candidate for spin injection into monolayer MoS_2.

Monolayer transition metal dichalcogenides, especially MoS_2, have promising prospects in many fields due to their exotic electronic, optical, chemical and thermal properties[1–4]. Unlike gapless graphene, monolayer MoS_2 has a direct optical band gap of 1.8 eV[5,6], which is key for field effect transistors, photodetectors and electroluminescent devices[7–9]. On the other hand, the low electron mobility hampers high performance applications. Interfaces often are more crucial to nanoelectronics than the involved semiconductors themselves[10,11]. Based on density functional theory, Gan *et al.* have shown that the chemical bonds formed at the MoS_2/TiC interface result in conductive MoS_2[12] and Feng *et al.* have predicted that the interfacial hybridization in Fe_4N/MoS_2 superlattices results in magnetic MoS_2[13]. Pb, Au and Ag contacts to monolayer MoS_2 can be used to realize good electron injection[14]. Popov *et al.*, on the other hand, have observed that Au is rather inefficient for electron injection and have proposed Ti as alternative electrode material[15]. Moreover, Chen *et al.* have demonstrated a *n*-type Schottky-barrier for the contact between monolayer MoS_2 and Ir(111), Pd(111), or Ru(0001)[16].

Clearly, interfaces between semiconductors and metals are critical for future electronic devices based on this new class of materials. In particular, injection of spin-polarized charge from ferromagnets may have a significant technological impact in the area of spintronics. Gd is one of the four room-temperature ferromagnetic metals (Curie temperature 293 K; the others being Fe, Co, and Ni). A significant enhancement of the Curie temperature by 29% has been found experimentally at the Gd(0001) surface[17]. In contrast to transition metals, the ferromagnetic order generated by the localized Gd 4*f* electrons also polarizes the conduction electrons (Gd 5*d* and 6*s*), leading to a large magnetic moment of 7.63 μ_B/Gd[18]. Moreover, Gd crystallizes in the hcp structure with less than 1% lattice mismatch to MoS_2 and has a low work function of 3.1 eV[19], thus being able to efficiently inject electrons into the conduction band of MoS_2. For these reasons, we investigate in the present work, the electronic structure of interfaces between two-, four- and six-layer Gd(0001) and monolayer MoS_2 by density functional theory, demonstrating great potential for spin injection.

Methods

Our first-principles calculations are performed using the projector-augmented wave method as implemented in the Vienna *Ab-initio* Simulation Package[20,21]. For the exchange-correlation potential we use the generalized gradient approximation (GGA) of Perdew, Burke and Ernzerhof[22]. Due to strong on-site Coulomb repulsion of the localized Gd 4*f* electrons, the rotationally invariant GGA+*U* method is employed with $U = 7.7$ eV and $J = 0.7$ eV[23]. The two-layer Gd/MoS_2 interface is also studied taking into account the spin-orbit coupling (GGA+SOC). In all calculations the Gd 5*s*, 5*p*, 6*s*, 5*d*, and 4*f* orbitals are treated as valence states, a Γ-centered $4 \times 4 \times 1$ *k*-grid is employed, and the plane wave energy cutoff is set to 600 eV. Furthermore, the convergence criterium for the total energy is chosen to be 10^{-5} eV. The surface unit cell of Gd(0001) has $p(3 \times 3)$ periodicity with experimental lattice constant 10.89 Å[24], while the surface unit cell of monolayer MoS_2 has $2\sqrt{3} \times 2\sqrt{3}$ R30° periodicity with experimental lattice constant 10.98 Å[25]. Thus, the mismatch amounts only to 0.83%. The cell volume is relaxed and the ionic positions are optimized, using the conjugated gradient method, until the Hellmann-Feynmann forces on each atom are reduced to less than 0.01 eV/Å. A 15 Å thick vacuum layer ensures decoupling in the slab geometry. Because of strong chemical bonding between Gd(0001) and monolayer MoS_2, van der Waals forces are not taken into account.

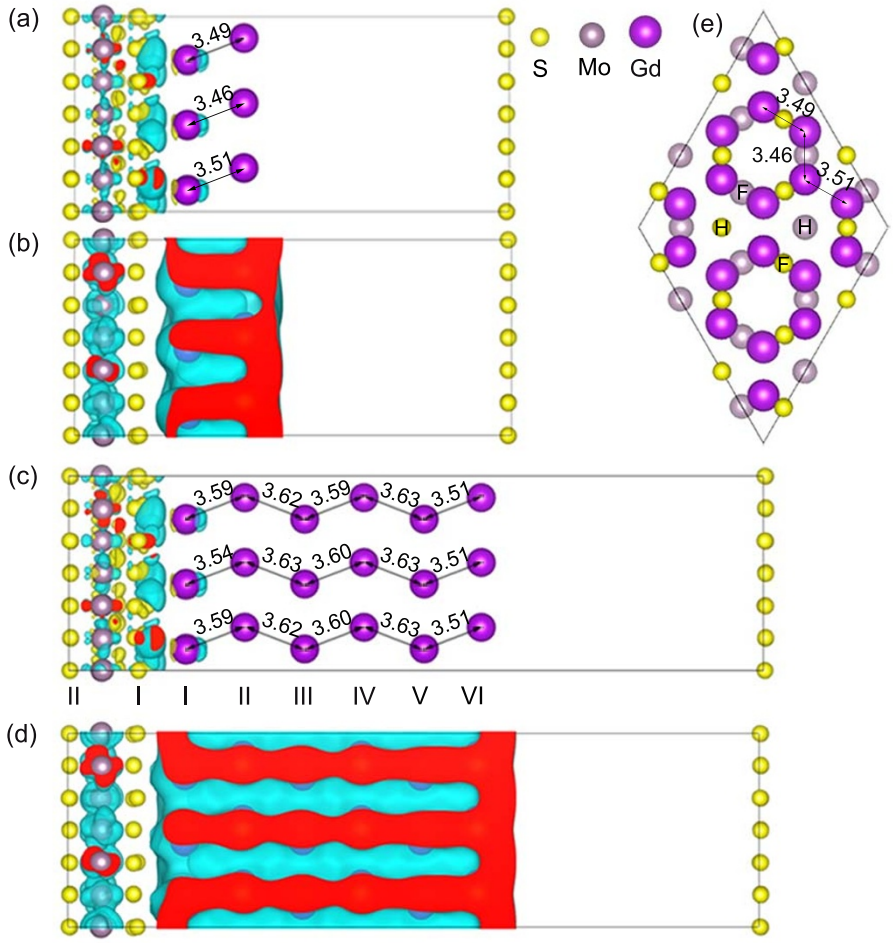

Figure 1 | (a, c) Side view of the charge density difference due to the interaction at the two- and six-layer Gd/MoS_2 interfaces. The cyan and yellow isosurfaces (±0.003 e/Å^3) represent accumulation and depletion of electrons, respectively. (b, d) Side view of the spin density difference for the two- and six-layer Gd/MoS_2 interfaces. The isosurface value is 0.002 e/Å^3. Red color indicates cuts through the isosurface. (e) Top view of the optimized two-layer Gd/MoS_2 interface.

Results and Discussion

Bulk MoS_2 has a layered 2*H* structure with space group $P6_3mmc$ (D_{6h} point group). The trigonal prismatic coordination of the bulk is maintained in monolayer MoS_2, whereas the symmetry is reduced to $P\bar{6}m2$ (D_{3h} point group) due to a loss of inversion symmetry. Gd crystallizes in a hcp structure with space group $P6_3mmc$. The optimized geometries of the interfaces between two- and six-layer Gd and monolayer MoS_2 are shown in Fig. 1. The results for the interface between four-layer Gd and monolayer MoS_2 turn out to be very similar to those of the six-layer system and thus are not further discussed in the following. According to Fig. 1(e), three S and Mo atoms in each layer sit above the hexagonal (H) hollow sites and nine S and Mo atoms are located above face-centered (F) hollow sites. The optimized lattice constants of Gd and MoS_2 are 3.65 and 3.18 Å, respectively, whereas for both the two- and six-layer Gd/MoS_2 interfaces we obtain 11.03 Å (3.68 and 3.18 Å for Gd and MoS_2). This means that there is almost no strain. In order to quantify the interaction strength between Gd and MoS_2, we calculate the binding energy $E_B = E_I - E_M - E_{Gd}$, where E_I, E_M, and E_{Gd} represent the total energies of the Gd/MoS_2 interface, monolayer MoS_2, and the Gd slab, respectively. We obtain per surface Gd atom values of −0.62 and −0.64 eV for the two- and six-layer Gd/MoS_2 interfaces, reflecting substantial bonding. The distance between the $S_{I,F}$ (the first index refers to the layer and the second to the site) and Mo_F atoms, respectively, and their nearest Gd neighbors is 2.77 and 4.23 Å (2.76 and 4.21 Å) in the two-layer (six-layer) Gd/MoS_2 interface, whereas the corresponding distance for the $S_{I,H}$ and Mo_H atoms is larger, namely, 3.17 and 4.69 Å (3.14 and 4.67 Å).

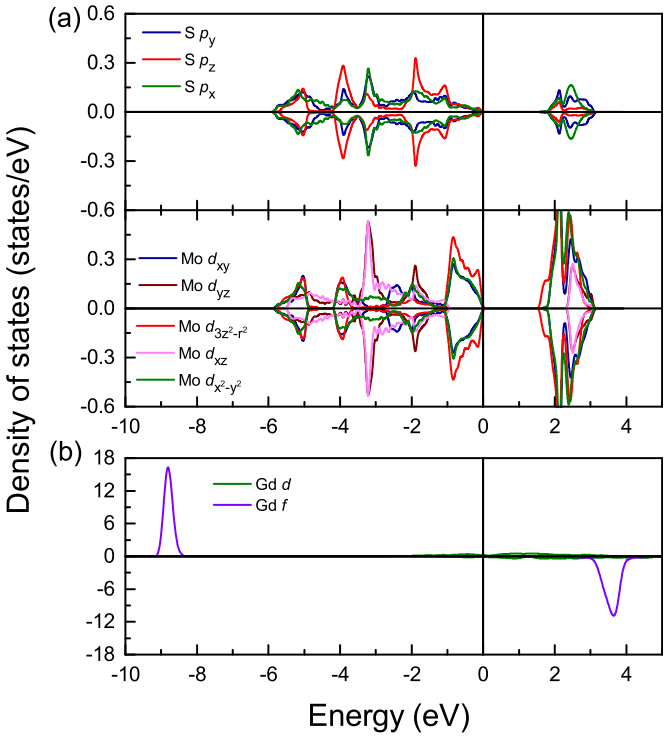

Figure 2 | **DOS of (a) the Mo and S atoms in pristine monolayer MoS_2 and (b) the Gd atoms in bulk Gd.**

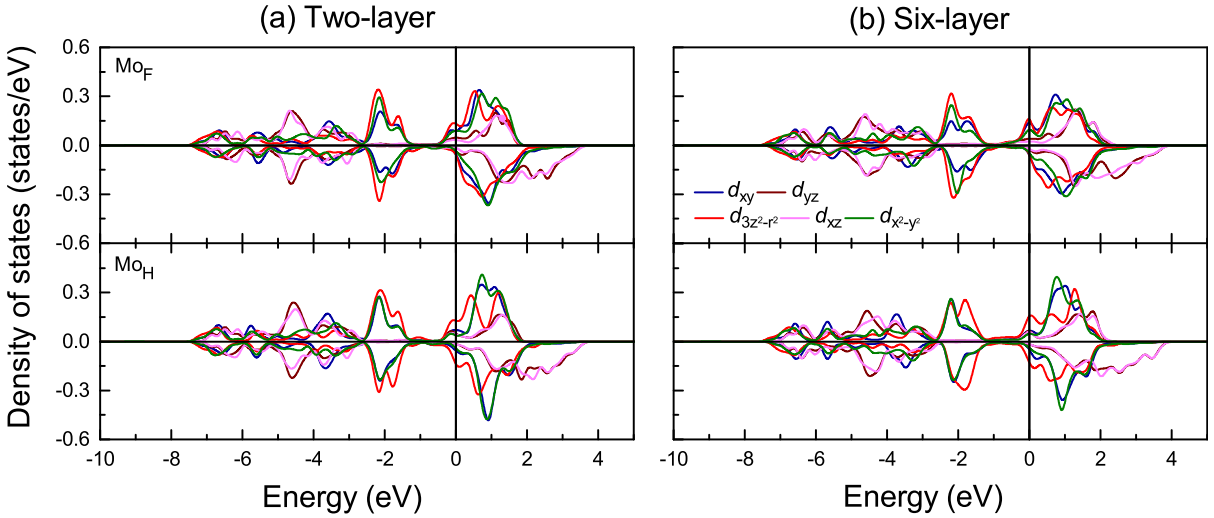

Figure 3 | **DOS of the Mo atoms at the F and H sites for the two- and six-layer Gd/MoS_2 interfaces.**

The density of states (DOS) of pristine monolayer MoS_2 is addressed in Fig. 2(a). The crystal-field splitting of the Mo 4*d* states in the trigonal prismatic environment of the S atoms is visible. Hybridization between the Mo $4d_{3z^2-r^2}$, d_{xy}, $d_{x^2-y^2}$ and S 3*p* states at the conduction and valence band edges is consistent with previous results[26]. Figures 3 and 4 give the DOSs obtained for the two- and six-layer Gd/MoS_2 interfaces. The majority spin Mo_F states at the Fermi energy (E_F) display high $4d_{3z^2-r^2}$, d_{xy}, and $d_{x^2-y^2}$ DOSs with d_{yz} and d_{xz} admixtures, while the minority spin DOSs are small. The majority spin Mo_H DOS at E_F is slightly larger than the minority spin DOS (mainly $d_{3z^2-r^2}$ states, followed by d_{xy}, $d_{x^2-y^2}$ and d_{yz}, d_{xz} states). Furthermore, the broader peaks in Fig. 3(a) as compared to Fig. 3(b) reflect more dispersive bands in the two-layer Gd/MoS_2 interface. To illustrate the charge transfer, we show the charge density difference between the Gd/MoS_2 interfaces and the sum of the isolated Gd and MoS_2 subsystems in Figs. 1(a) and (c). Charge accumulates at the Mo atoms and in the Gd-S bond region. The Mo excess electrons populate majority spin states, resulting in enhanced Mo 4*d* magnetic

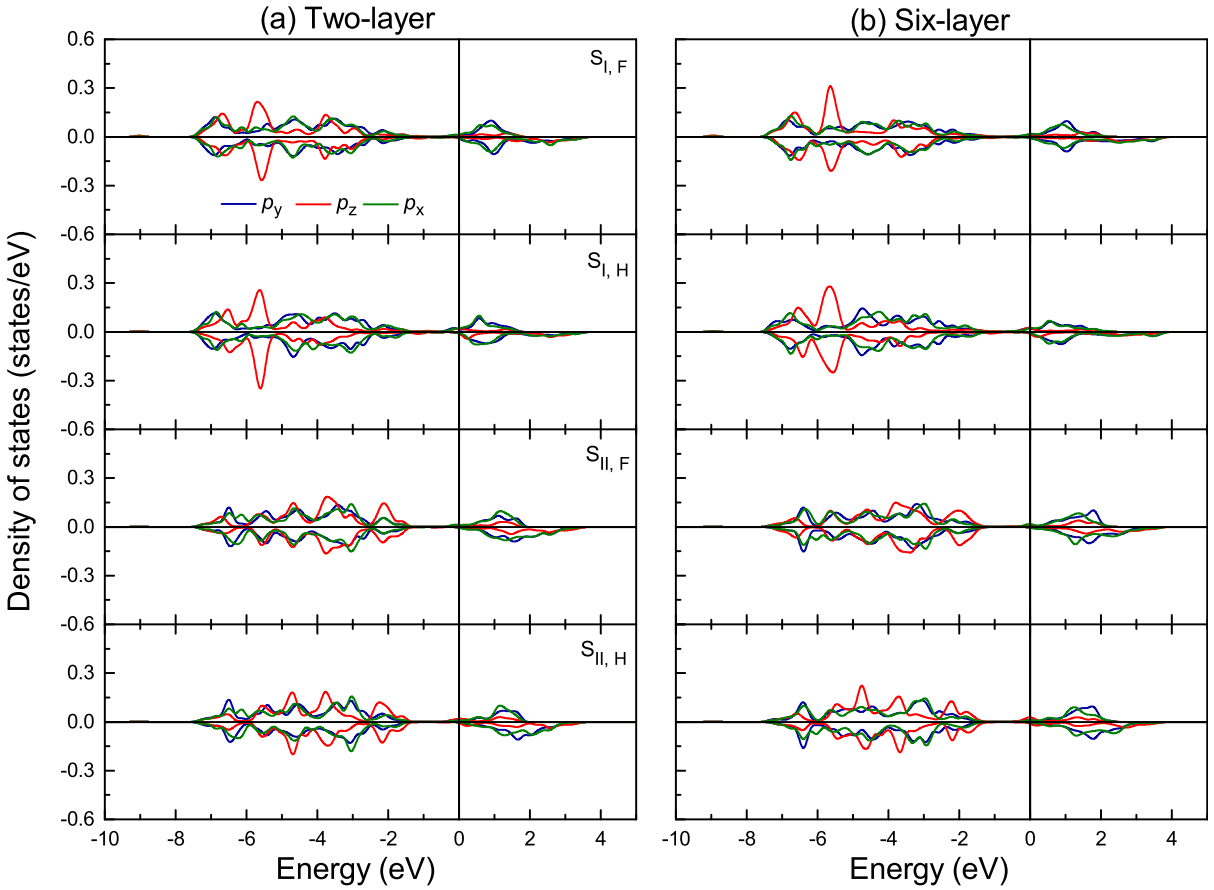

Figure 4 | **DOS of the S atoms at the F and H sites for the two- and six-layer Gd/MoS_2 interfaces.**

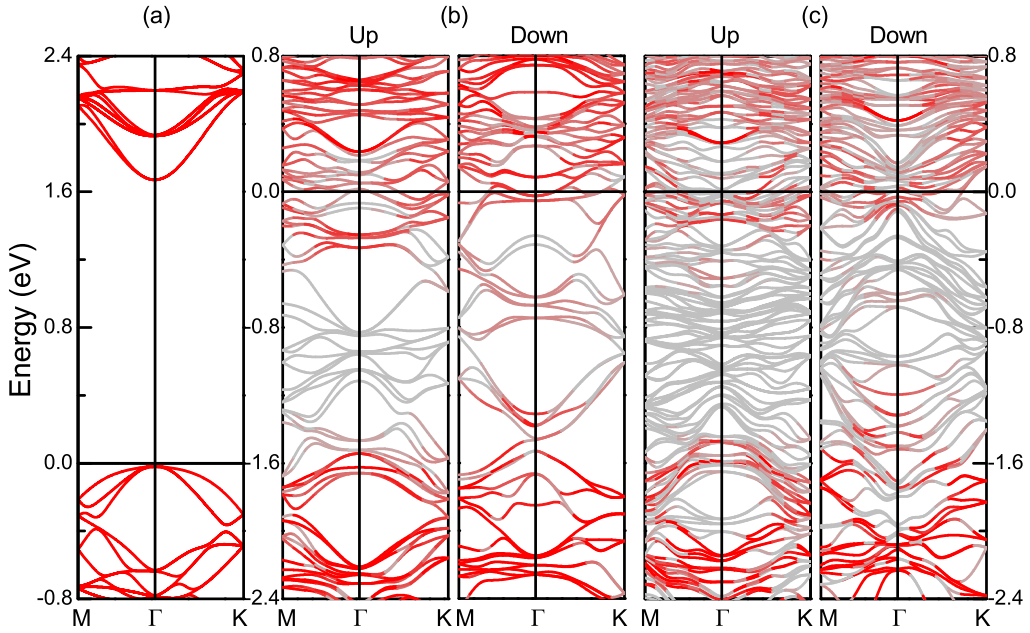

Figure 5 | Band structure of (a) pristine monolayer MoS_2 and (b, c) the two- and six-layer MoS_2 interfaces. $E_F = 0$ eV. The red lines correspond to the bands of monolayer MoS_2.

moments. Figure 4 demonstrates that for S_{II} the p_z DOS is larger than the p_x and p_y DOSs, similar to pristine monolayer MoS_2, at the valence band edge, while for S_I mainly the p_x and p_y orbitals contribute. This means that the Gd-S_{II} interaction is weak (large distance). Due to hybridization with the Gd 5*d* states (details later), some S *p* states show up at E_F, especially majority spin states, which leads to a tiny S magnetic moment (0.01 μ_B). It is worth noting that, due to the nonmagnetic nature of MoS_2, we have set the initial magnetic moments of S and Mo to zero in all calculations. The spatial extension of the spin density in MoS_2 induced by the contact to Gd is shown in Figs. 1(b) and (d). It mainly extends into the Mo region and is small for S (large change of the Mo DOS). We find that the Mo magnetic moments order ferromagnetically. The shorter Mo_F-Gd distance as compared to the Mo_H-Gd distance enhances the interaction so that Mo_F has a larger magnetic moment of about 0.12 and 0.15 μ_B (Mo_H: 0.07 and 0.10 μ_B) in the two- and six-layer Gd/MoS_2 interfaces, respectively.

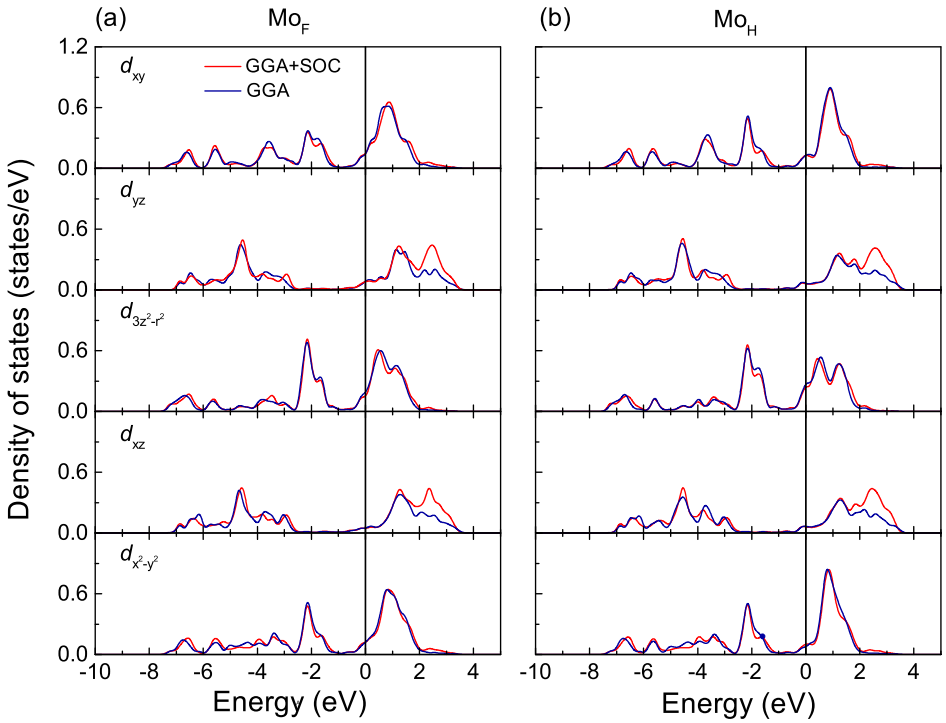

Figure 6 | DOS (sum of both spin channels) of the Mo atoms at the F and H sites for the two-layer Gd/MoS_2 interface: Comparison between the GGA and GGA+SOC methods. $E_F = 0$ eV.

Table 1 | Gd 5*d* and 4*f* magnetic moments (μ_B) in each layer of the two- and six-layer Gd/MoS_2 interfaces, as compared to bulk Gd

System	Layer	*d*	*f*
Bulk		0.4	7.0
Two-layer	I	0.3	7.0
	II	0.5	7.0
Six-layer	I	0.4	7.0
	II	0.4	7.0
	III	0.4	7.0
	IV	0.4	7.0
	V	0.4	7.0
	VI	0.5	7.0

Figure 5(a) shows a band gap of 1.6 eV for pristine monolayer MoS_2, consistent with previous GGA calculations[27]. In the combined systems, although the bands of MoS_2 hybridize with those of Gd they can still be identified, see the red color in Figs. 5(b) and (c). We find E_F 0.34 and 0.51 eV, respectively, above the conduction band edge for the majority and minority spin bands, making MoS_2 display a metallic character. Figs. 6(a) and (b) show the DOS for Mo_F and Mo_H in the two-layer Gd/MoS_2 interface as obtained by GGA+SOC in comparison to simple GGA. We find that the SOC has almost no influence, except for a slight reduction of the $d_{3z^2-r^2}$ DOS.

The distance between nearest neighbor atoms is 3.60 Å in bulk Gd, while the distances of nearest neighbor atoms in the interface and surface Gd layers, see Figs. 1(a, e) and (c), respectively, are smaller. The very short distance between layers V and VI in the six-layer Gd/MoS_2 interface points to a substantial surface relaxation. On the other hand, the distances in the subsurface, see Fig. 1(c), are larger than the bulk value. This variation is consistent with a contraction of the surface layer by 0.085–0.115 Å (~3–4%) and an expansion of the subsurface layer by 0.050–0.075 Å (~1.5–2.5%) as measured by low-energy electron diffraction[28,29].

In bulk Gd the unoccupied *f* states are located 3.6 eV above E_F and the occupied *f* states 8.8 eV below E_F, see Fig. 2(b), reflecting an exchange spin splitting of 12.4 eV. This value agrees with results of the full potential linear augmented plane wave method[30] and is close to the experimental value of 12 eV[31]. The fact that the Gd magnetic moment (7.43 μ_B) exceeds 7 μ_B suggests an induced polarization of other orbitals. We find magnetic moments of 0.02, 0.03 and 0.40 μ_B for the Gd *s*, *p*, and *d* states, which can be explained by the *s*-*f* exchange model[32]. The total Gd magnetic moments are enhanced in the surface Gd layers by 0.9% and 1.9% for the two- and six-layer Gd/MoS_2 interfaces, respectively, and reduced by 0.9% and 0.5% in the interface Gd layers. The magnetic moments of the different layers given in Table 1 show no effect for the *f* states; all changes are carried by the *d* states. The Gd *d* DOS in Fig. 7, in contrast to the bulk, shows majority spin states from −0.5 to 0.4 eV (from −0.2 to 0.2 eV) for the two-layer (six-layer) Gd/MoS_2 interface for the surface[33–37] (more pronounced) and interface Gd atoms. Moreover, a strong hybridization between the Gd *d*, Mo *d* and S *p* states appears near E_F (see Figs. 3, 4 and 7). The majority and minority spin Gd *d* DOSs at E_F are different because of an enhancement in the surface and a reduction in the interface Gd layers. In the other Gd layers the Gd magnetic moments are close to the bulk value of 7.43 μ_B. The Gd *f* DOSs of layers I and II, respectively, show downward shifts of 0.2 and 0.3 eV for the majority spin states and of 0.3 and 0.4 eV for the minority spin states, relative to the bulk Gd *f* states, where the different amplitude is due to the interaction with MoS_2 in layer I. The same is found for the I and VI layers in the six-layer Gd/MoS_2 interface, which is consistent with inverse photoemission spectroscopy[37], while for the II, III, IV, and V layers the shifts are very small. Gd core-level shifts can be attributed to the different chemical environments of the surface and interface atoms, thus being small in other layers.

Conclusion

We have investigated the geometry, electronic structure, and magnetism at the interface between Gd(0001) and monolayer MoS_2. Strong chemical bonds are formed and seriously modify the electronic states of MoS_2, especially at E_F. Interaction with the Gd *d* states shifts E_F into the conduction band and makes MoS_2 metallic. Large magnetic moments appear on the Mo atoms. Moreover, distinct surface/interface Gd *d* states are formed at E_F and a clear downward shift of the Gd *f* states is observed for both the surface and interface, whereas the Gd magnetic moments are enhanced at the surface but reduced at the interface.

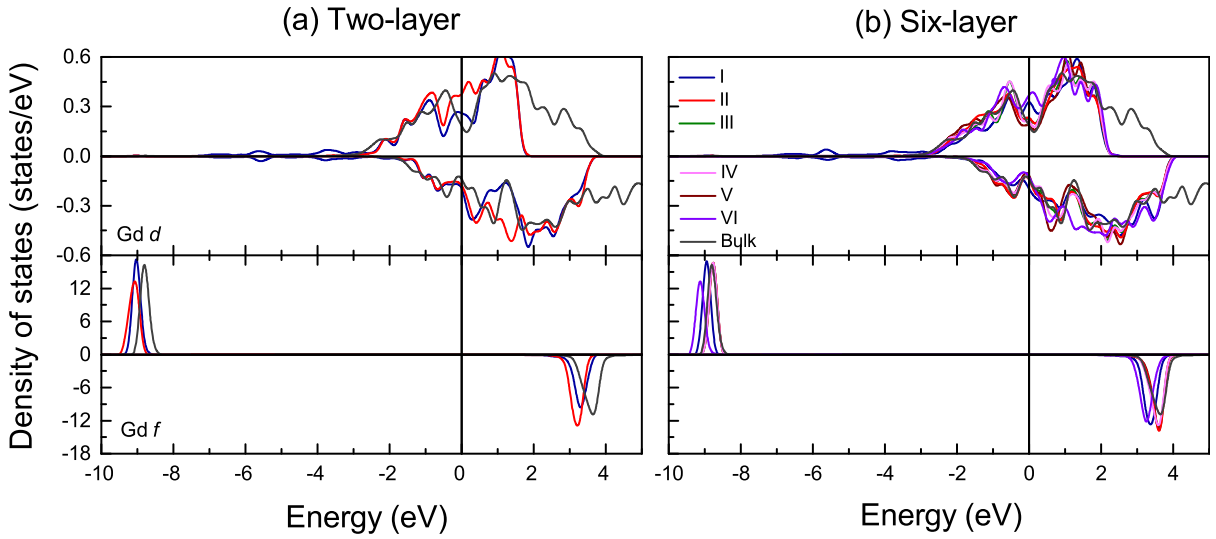

Figure 7 | DOS of the Gd atoms in the different atomic layers of the two- and six-layer Gd/MoS_2 interfaces. $E_F = 0$ eV.

1. Bertolazzi, S., Brivio, J. & Kis, A. Stretching and breaking of ultrathin MoS_2. *ACS Nano* **5**, 9703 (2011).
2. Wang, Q. H. *et al.* Electronics and optoelectronics of two-dimensional transition metal dichalcogenides. *Nature Nanotech.* **7**, 699 (2012).
3. Li, T. Ideal strength and phonon instability in single-layer MoS_2. *Phys. Rev. B* **85**, 235407 (2012).
4. Xiao, D. *et al.* Coupled spin and valley physics in monolayers of MoS_2 and other group-VI dichalcogenides. *Phys. Rev. Lett.* **108**, 196802 (2012).
5. Mak, K. F. *et al.* Atomically thin MoS_2: A new direct-gap semiconductor. *Phys. Rev. Lett.* **105**, 136805 (2010).
6. Lee, H. S. *et al.* MoS_2 nanosheet phototransistors with thickness-modulated optical energy gap. *Nano Lett.* **12**, 3695 (2012).
7. Radisavljevic, B. *et al.* Single-layer MoS_2 transistors. *Nature Nanotech.* **6**, 147 (2011).
8. Splendiani, A. *et al.* Emerging photoluminescence in monolayer MoS_2. *Nano Lett.* **10**, 1271 (2010).
9. Eda, G. *et al.* Photoluminescence from chemically exfoliated MoS_2. *Nano Lett.* **11**, 5111 (2011).
10. Leonard, F. & Talin, A. A. Size-dependent effects on electrical contacts to nanotubes and nanowires. *Phys. Rev. Lett.* **97**, 026804 (2006).
11. Lin, Y. F. & Jian, W. B. The impact of nanocontact on nanowire based nanoelectronics. *Nano Lett.* **8**, 3146 (2008).
12. Gan, L. Y., Zhao, Y. J., Huang, D. & Schwingenschlogl, U. First-principles analysis of MoS_2/Ti_2C and MoS_2/Ti_2CY_2 (Y = F and OH) all-2D semiconductor/metal contacts. *Phys. Rev. B* **87**, 245307 (2013).
13. Feng, N. *et al.* Magnetism by interfacial hybridization and *p*-type doping of MoS_2 in Fe_4N/MoS_2 superlattices: A First-principles study. *ACS Appl. Mater. Interfaces* **6**, 4587 (2014).
14. Gong, C. *et al.* Metal contacts on physical vapor deposited monolayer MoS_2. *ACS Nano* **7**, 11350 (2013).
15. Popov, I., Seifert, G. & Tomanek, D. Designing electrical contacts to MoS_2 monolayers: A computational study. *Phys. Rev. Lett.* **108**, 156802 (2012).
16. Chen, W. *et al.* Tuning the electronic and chemical properties of monolayer MoS_2 adsorbed on transition metal substrates. *Nano Lett.* **13**, 509 (2013).
17. Weller, D. *et al.* Observation of surface-enhanced magnetic order and magnetic surface reconstruction on Gd(0001). *Phys. Rev. Lett.* **54**, 1555 (1985).
18. Jensen, J. & Mackintosh, A. R. Rare earth magnetism (Clarendon Press, Oxford, 1991).
19. Michaelson, H. B. The work function of the elementa and its periodicity. *J. Appl. Phys.* **48**, 4729 (1977).
20. Kresse, G. & Joubert, D. From ultrasoft pseudopotentials to the projector augmented-wave method. *Phys. Rev. B* **59**, 1758 (1999).
21. Blochl, P. E. Projector augmented-wave method. *Phys. Rev. B* **50**, 17953 (1994).
22. Perdew, J. P., Burke, K. & Ernzerhof, M. Generalized gradient approximation made simple. *Phys. Rev. Lett.* **77**, 3865 (1996).
23. Harmon, B. N. *et al.* Calculation of magneto-optical properties for 4*f* systems: LSDA+ Hubbard *U* results. *J. Phys. Chem. Solids* **56**, 1521 (1995).
24. Petkov, V. B. *et al.* Structure of nanocrystalline meterials using atomic pair distribution function analysis: Study of $LiMoS_2$. *Phys. Rev. B* **65**, 092105 (2002).
25. Banister, J. R., Legvold, S. & Spedding, F. H. Structure of Gd, Dy, and Er at low temperatures. *Phys. Rev.* **94**, 1140 (1954).
26. Mattheiss, L. F. Band structures of transition-metal-dichalcogenide layer compounds. *Phys. Rev. B* **8**, 3719 (1973).
27. Ramasubramaniam, A. Large excitonic effects in monolayers of molybdenum and tungsten dichalcogenides. *Phys. Rev. B* **86**, 115409 (2012).
28. Quinn, J., Li, Y. S., Jona, F. & Fort, D. Atomic structure of a Gd(0001) surface. *Phys. Rev. B* **46**, 9694 (1992).
29. Giergiel, J. *et al.* Surface structure of epitaxial Gd(0001) films on W(110) studied by quantitative LEED analysis. *Phys. Rev. B* **51**, 10201 (1995).
30. Abdelouahed, S., Baadji, N. & Alouani, M. Electronic structure and x-ray magnetic circular dichroism of gadolinium beyond the local spin density approximation. *Phys. Rev. B* **75**, 094428 (2007).
31. Dowben, P. A., McIlroy, D. N. & Li, D. in Handbook on the Physics and Chemistry of Rare Earths (Elsevier, North-Holland, 1997). Vol. 24, p. 1–46.
32. Nolting, W., Dambeck, T. & Borstel, G. Temperature-dependent electronic structure of Gadlinium. *Phys. B: Condens. Matter* **94**, 409 (1994).
33. Shick, A. B., Pickett, W. E. & Fadley, C. S. Electron correlation effects and magnetic ordering at the Gd(0001) surface. *Phys. Rev. B* **61**, 9213 (2000).
34. Li, D. Q., Zhang, J. D., Dowben, P. A. & Onellion, M. Temperature-dependent electronic structure in a localized-magnetic-moment system gadolinium. *Phys. Rev. B* **45**, 7272 (1992).
35. Li, D. Q. *et al.* Angle-resolved photoemission evidence for a Gd(0001) surface state. *J. Magn. Magn. Mater.* **99**, 85 (1991).
36. Li, D. Q. *et al.* Fabricating magnetic CoNiC thin film alloys by organometallic chemical vapor deposition. *J. Appl. Phys.* **70**, 6062 (1991).
37. Li, D. Q., Dowben, P. A., Ortega, J. E. & Himpsel, F. J. Unoccupied surface electronic structure of Gd(0001). *Phys. Rev. B* **49**, 7734 (1994).

Acknowledgments

The work was supported by the National Natural Science Foundation of China (51171126), the Key Project of the Natural Science Foundation of Tianjin City (12JCZDJC27100), the Program for New Century Excellent Talents in University (NCET-13-0409) and the Scientific Research Foundation for the Returned Overseas Chinese Scholars, State Education Ministry. Research reported in this publication was supported by the King Abdullah University of Science and Technology (KAUST).

Author contributions

X.Z. and W.M. designed the outline of the manuscript and wrote the main text. U.S. gave many good suggestions and contributed detailed discussions and revisions. X.W. and Y.C. contributed detailed discussions and revisions. All authors reviewed the manuscript.

Additional information

Competing financial interests: The authors declare no competing financial interests.

How to cite this article: Zhang, X., Mi, W., Wang, X., Cheng, Y. & Schwingenschlögl, U. The Interface between Gd and Monolayer MoS_2: A First-Principles Study. *Sci. Rep.* **4**, 7368; DOI:10.1038/srep07368 (2014).